Hindawi
International Journal of Antennas and Propagation
Volume 2019, Article ID 6087039, 13 pages
https://doi.org/10.1155/2019/6087039

Research Article

UWB Metamaterial-Loaded Antenna for C-Band Applications

Parul Dawar,[1] **N. S. Raghava**,[2] **and Asok De**[2]

[1]*Guru Tegh Bahadur Institute of Technology, GGSIPU, Department of ECE, Delhi, India*
[2]*Delhi Technological University, Department of ECE, Delhi, India*

Correspondence should be addressed to Parul Dawar; paru.dawar@gmail.com

Received 17 January 2018; Revised 11 June 2018; Accepted 16 October 2018; Published 6 January 2019

Academic Editor: Luciano Tarricone

A novel metamaterial-inspired patch antenna is proposed, wherein a 2-segment SRR Labyrinth metamaterial is embedded inside the antenna substrate. It is observed that upon incorporation, the bandwidth widens to around 600% and VSWR improves by approx. 1.5% and the antenna is miniaturized by 400%. The Nicolson-Ross-Weir (NRW) method has been used to retrieve the material parameters from transmission and reflection coefficients.

1. Introduction

Nowadays, the trend is developing devices for wireless communication systems which have inherent high bandwidth, gain, and multiresonance. Rectangular microstrip patch antenna, i.e., RMPA, is not a good candidate as it has a narrow bandwidth, in sufficient gain and directive properties. Thus, various optimization techniques have been introduced to make patch antenna a successful candidate in wireless communication applications.

With the development of metamaterials came the concept of attaining altered behaviour of electromagnetic radiations, i.e., μ, ε, and η, thus providing a better solution for attaining enhanced antenna's performance. "Metamaterials" (MTMs) are engineered to modify the bulk permeability and/or permittivity of the medium [1]. It is realized by placing, periodically, structures that alter the material parameters, with elements of size less than the wavelength of the incoming electromagnetic wave. It results in "meta," i.e., "altered," behaviour or behaviour unattainable by natural materials. In this paper, a novel antenna structure is proposed with enhanced performance parameters and miniaturization using metamaterial.

2. Metamaterial Design

The study of microstrip patch antennas has made progress in recent years. Compared with conventional antennas, microstrip patch antennas have more advantages and better prospects. They are lighter in weight and have low volume, low cost, low profile, small dimension, ease of fabrication, and conformity. Moreover, the microstrip patch antennas can provide dual and circular polarizations, dual-frequency operation, frequency agility, broad bandwidth, feed line flexibility, and beam scanning omnidirectional patterning. In literature, the following structures have been discussed to improve the bandwidth of the patch antenna:

(1) Defected ground structure

(2) Electromagnetic band-gap structures

(3) Metamaterials

The basic element of DGS is a resonant gap or slot in the ground metal. It helps in the reduction of surface waves, but the disadvantage of using DGS is reduction in antenna efficiency due to back lobe formation. EBGs are a periodic arrangement of dielectric or metallic elements in one-, two-, or three-dimensional manner. By introducing the structure, the surface waves are reduced as the ground/patch is loaded with inductance and capacitance, but the disadvantage of using EBG is that the area of the antenna is increased. By using metamaterials, the antenna's bandwidth is enhanced and also multiresonance may be observed by studying its response to the incident EM wave. The behaviour of the metamaterial unit cell can be studied in respect of

polarization when the incident electromagnetic wave is perpendicular to it, which is depicted by a resonating curve between its permittivity and permeability with respect to frequency. In negative index materials, phase and energy velocities follow the left hand rule. In order to observe the negative group and phase velocities, a positive index material slab is embedded with negative index material in the middle as shown in Figure 1.

The group velocity follows the right hand rule and propagates towards the right irrespective of the medium as shown in Figure 1. When ϵ and μ both are negative, phase velocity follows the left hand rule but the direction of propagation is reversed. This leads to the formation of "backward wave" in materials with negative refraction. However, if either ϵ or μ is negative, then evanescent waves occur. Many structures have been analyzed in literature [3–10] to establish this theory of left-handedness and composite material concept. This analysis of various 2D and 3D structures is based on several factors like spacing, size, arrangement, shapes, compositions, density, or materials used. In Figure 2, a generic view of metamaterials made with periodic inclusions resulting in an effective bulk permittivity and permeability is shown.

3. Evolution of the Shape of the Proposed Metamaterial

In literature [11, 12], the geometry of the SRR consists of two square shape rings with their slit displaced by 180° or 2π as shown in Figure 3.

The split or gap (g) of SR is 0.8 mm wide, the ring width (t) is 35 microns, and substrate thickness (h) is 1.6 mm. The spacing (s) between the nth and $(n+1)$th turn is 0.4 mm. The SRR is printed on a FR4 substrate having relative permittivity, εr, as 4.4.

A unit cell is designed with the above dimensions, and the simulation result is shown in Figure 4.

By introducing one split each in respective arms, capacitances in gaps are introduced. As per the equivalent circuit, the more the gaps, the more will be the Cg introduced in parallel, which means reduced effective capacitance. Thus, the resonant frequency increases. Therefore, resonant frequency is calculated to be 2.08 GHz.

If the square ring is single, i.e., only the outer ring is considered with a single split, then the resonant frequency increases. This is because the capacitance reduces as there is no coupling between the rings. The resonant frequency is calculated to be 2.83 GHz.

Therefore, the physical explanation is in coherence with the theoretical explanation of the change in resonant frequency of different configurations of square SRR. The above unit cells are designed, and the simulated result is shown in Figure 5.

Thus, an analysis can be made on the two different shapes of the SRR, i.e., circular and square, with single split and double split each keeping the outer perimeter same. A curve in Figure 6 summarizes the inferences.

The above curve has been proved using physical analysis. Also, the reason for the lower resonant frequency in square

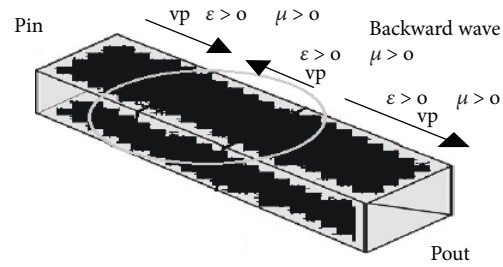

Figure 1: Antiparallel phase and group velocity if waveguide is made of metamaterial.

shape SRR than in circular SRR can be justified from the current distribution as shown in Figure 7.

The square SRR has greater current density than the circular one. It means more inductance, hence the lower resonant frequency. Thus, different shapes can be derived from these basic two shapes, i.e., square SRR and circular SRR. The advantages of the changing shape of the split-ring resonator from primitive circular shape to square are:

(1) Better degree of control: a circular SRR has a radius and width of the ring as the parameters that can be varied to control the constitutive material parameters of the medium. However, using square shape SRR, an extra variable parameter is available. Thus, a better degree of control is achievable using length, breadth, and width of the ring in square SRR.

(2) Better candidate as metamaterial: using a square shape SRR, the resonant frequency of the unit cell is reduced. Thus, (a/λ), which is the ratio of the unit cell dimension to the wavelength of operation, increases. This makes the metamaterial a better candidate over circular SRR.

The epsilon-negative group (i.e., negative permittivity) of metamaterials, shown in Figure 2(a), provided an appreciable increase in bandwidth, which are analogous to a medium consisting of thin wires arranged in a periodic array [12]. It is also observed that the permittivity ϵ varies with frequency ω of operation of the unit cell as presented in Equation (1):

$$\varepsilon(\omega) = 1 - \frac{\omega p^2}{\omega(\omega + i\gamma)}, \tag{1}$$

where ω_p is the plasma frequency and γ is a damping term.

In Equation (1), if the plasma frequency is less than the operating frequency, then the permittivity becomes negative.

In this paper, the mu-negative group (i.e., negative permeability) metamaterial shown in Figure 2(b) is explored as a 2-segment labyrinth metamaterial. If the rod and ring materials are combined, a left-handed material [13] is formed having simultaneously negative ϵ and μ. The reason is that the wire strips affect the ϵ and the split-ring resonators (SRRs) alter the μ of the medium. Thus, a frequency-dependent negative material with both the parameters being negative is obtained.

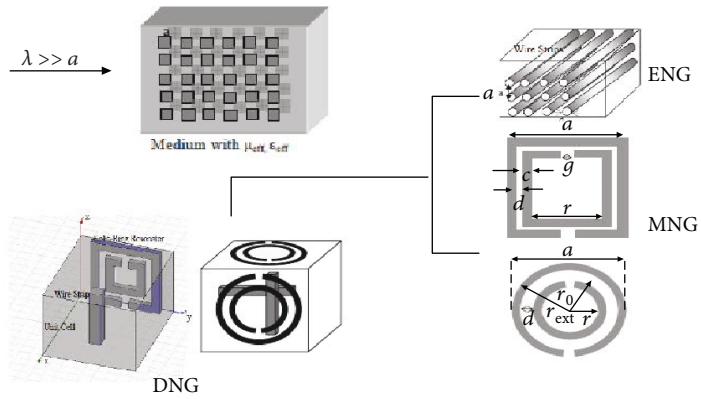

Figure 2: Generic view of a host medium with periodically placed structures constituting a metamaterial, ENG (epsilon-negative group), MNG (mu-negative group), and DNG (double-negative group).

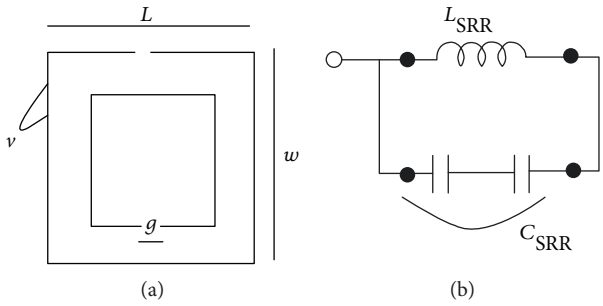

Figure 3: Geometry of square SRR and its equivalent circuit.

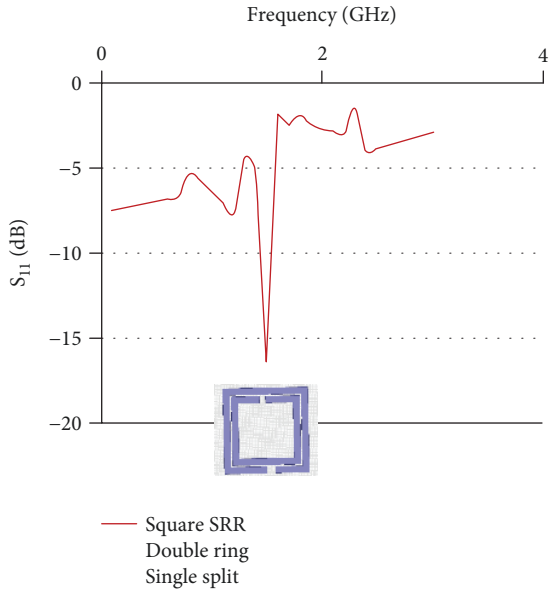

Figure 4: Unit cell analysis of square SRR.

4. 2-Segment SRR Metamaterial

The evolution of square SRR into double-split SRR has been explained in the previous section. The 2-segment labyrinth metamaterial design is as shown in Figure 8. The values of the design parameters are conductivity ρ_s of 0.034×10^{-3}

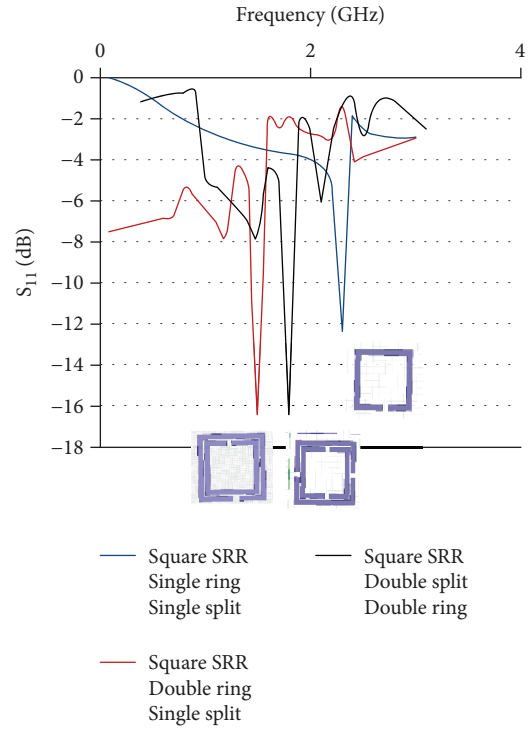

Figure 5: Unit cell analysis of different configurations of square SRR.

Ωm, side length l of the external ring of 10.2 mm, width of the strips u of 1.8 mm, separation between two adjacent strips s of 0.4 mm, gap width g of 0.8 mm, and thickness t of the conducting metallic inclusions of 0.16 μm.

This metamaterial is embedded in the middle of the antenna's substrate such that the center of patch coincides with the center of the metamaterial. The structure is then simulated using HFSS software. The top view of the 2-segment SRR metamaterial RMPA is shown in Figure 9.

4.1. Mathematical Analysis of the 2-Segment SRR Metamaterial. A 2-segment labyrinth metamaterial discussed in the previous section in Figure 8 is analyzed theoretically, and the results are compared with mathematical analysis

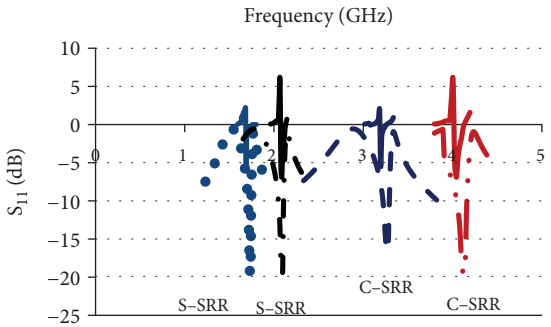

Figure 6: Comparison of circular (*C*) and square SRR (*S*) resonant frequency.

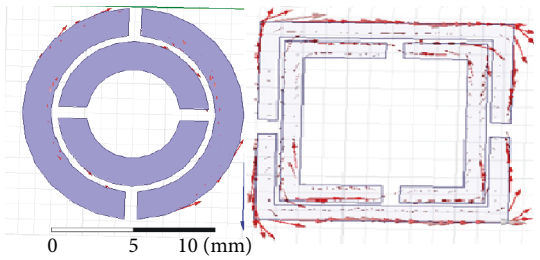

Figure 7: Current distribution in circular and square SRR.

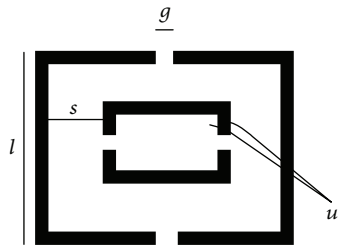

Figure 8: 2-Segment SRR metamaterial.

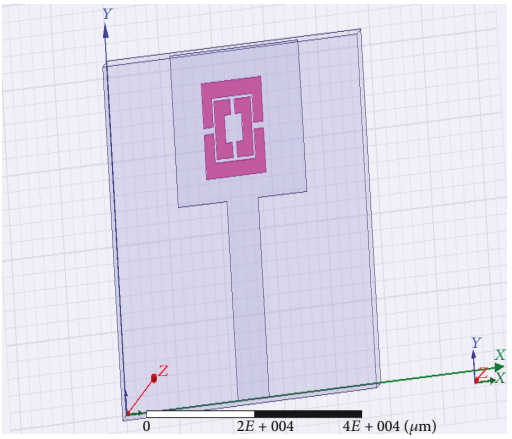

Figure 9: Top view of 2-segment SRR metamaterial RMPA.

using an equivalent circuit in this section. The Nicholson-Ross-Weir (NRW) method [14, 15] is used to retrieve or extract the parameters to observe the permeability region of SRR. The metamaterial in the dielectric substrate is bounded

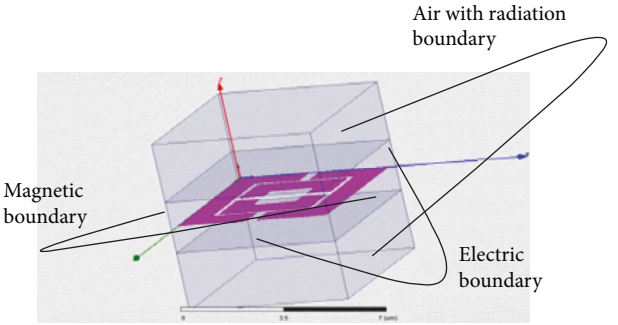

Figure 10: 2-Segment MTM: unit cell for parameter extraction.

by a box on either side as shown in Figure 10 and has air and radiation boundary on the top and bottom.

Using the NRW equation ((2)), the resonance in permeability is obtained as shown in Figure 6. The variables of Equation (2) are defined, and values of μ_r and ϵ_r are derived through the HFSS software.

$$\begin{bmatrix} \mu_r = \dfrac{2}{jK_0 d} \cdot \dfrac{1 - V_2}{1 + V_2} \\ \varepsilon_r = \dfrac{2}{jK_0 d} \cdot \dfrac{1 - V_1}{1 + V_2} \end{bmatrix}, \tag{2}$$

where k_0 is a wave number, d is the thickness of the substrate, and V_1 and V_2 are the composite terms to represent the addition and subtraction of scattering parameters and are given by Equation (3):

$$\begin{bmatrix} V_1 = S_{21} - S_{11} \\ V_2 = S_{21} + S_{11} \end{bmatrix} \tag{3}$$

Using Equations (2) and (3), the resonance in permeability is obtained in Figure 11.

It is observed in Figure 11 that the magnetic resonance is obtained at 4.2 GHz. The resonance in permeability is because a 2-segment SRR MTM has magnetic properties due to internal inductances and capacitances. Thus, the 2-segment labyrinth metamaterial behaves as a mu-negative group (MNG) having negative permeability over some frequency region [2].

The equivalent circuit of the above unit cell can be drawn as shown in Figure 12. It can be made as a combination of parallel RC and series of RL components using transmission line theory. The inductance L is taken for unit length of the loop, and capacitance C can be taken for the gap in the loop. The series resistance R_1 describes the losses in the conductor and the shunt resistance R_2 for the losses in the dielectric.

The inductance per unit length of the loop (L) is given by Equation (4) [16]:

$$L = \frac{\mu 0}{2} \frac{lavg}{4} 4.86 \left[\ln \left(\frac{0.98}{\rho} \right) + 1.84\rho \right], \tag{4}$$

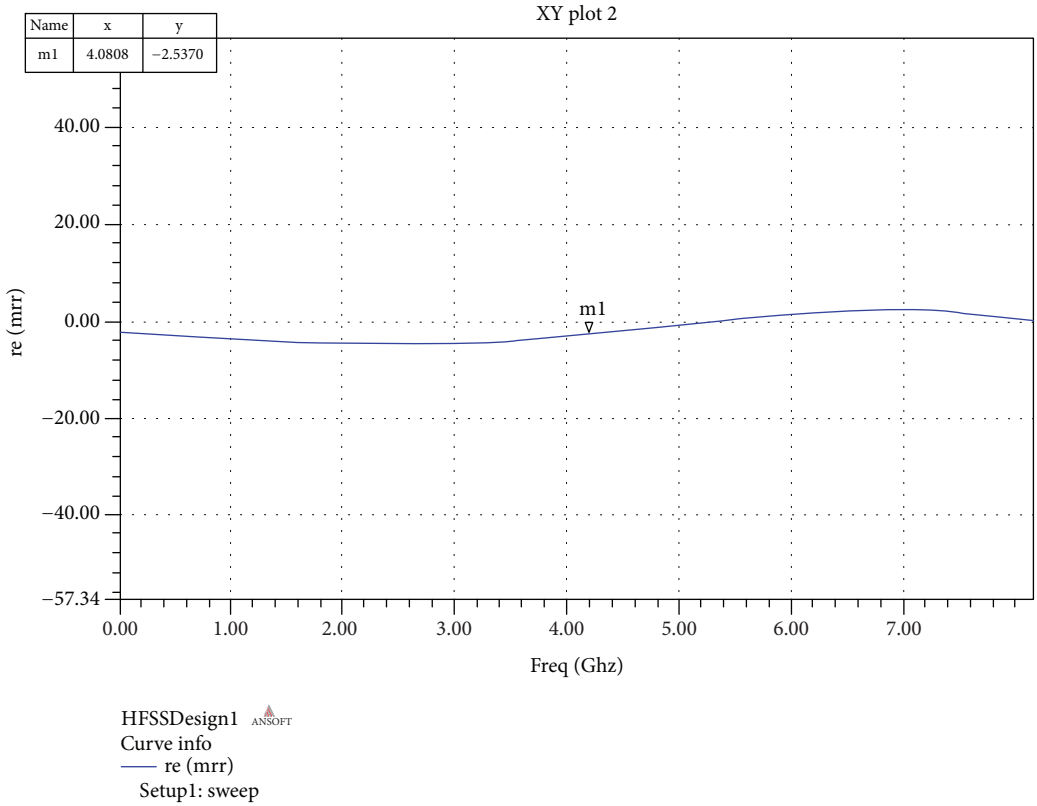

Figure 11: Resonance in permeability.

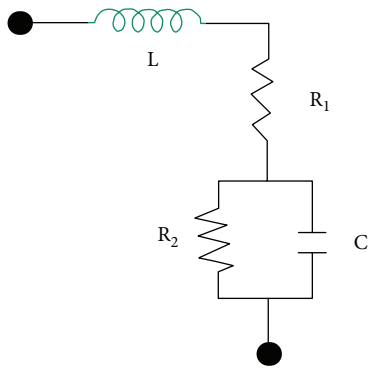

Figure 12: Equivalent circuit of 2-segment SRR metamaterial.

where μ_0 is the vacuum permeability and l_{avg} is the average strip length and is calculated over all the rings using Equation 5:

$$l\text{avg} = 4[l - (N-1)(u+s)], \tag{5}$$

where ρ is the filling ratio of the SRR between the cross-links.

Using Equation (5), l_{avg} is calculated as 36 mm. Therefore, substituting it in Equation (4), inductance L is obtained as 3×10^{-6} H.

Similarly, the capacitance of the gap (C) is given by Equation (6):

$$C = \frac{N-1}{2}[2l - (2N-1)(w+s)]C_0, \tag{6}$$

where C_0 is the per-unit-length capacitance between two parallel strips and is given by Equation (7):

$$C0 = \varepsilon 0 \varepsilon r^{\text{sub}} \frac{K\left(\sqrt{1-k^2}\right)}{K(k)}, \tag{7}$$

$\varepsilon r^{\text{sub}}$ is the effective relative permittivity related to the dielectric filling of the substrate and is given by Equation (8):

$$\varepsilon r^{\text{sub}} = 1 + \frac{2}{\pi} \text{art}g\left[\frac{h}{2\pi(w+s)}\right](\varepsilon r - 1), \tag{8}$$

where

u is the width of the segment of MTM
s is the separation between the 2 segments of MTM
h is height of substrate of MTM
$\varepsilon 0$ is the vacuum permittivity

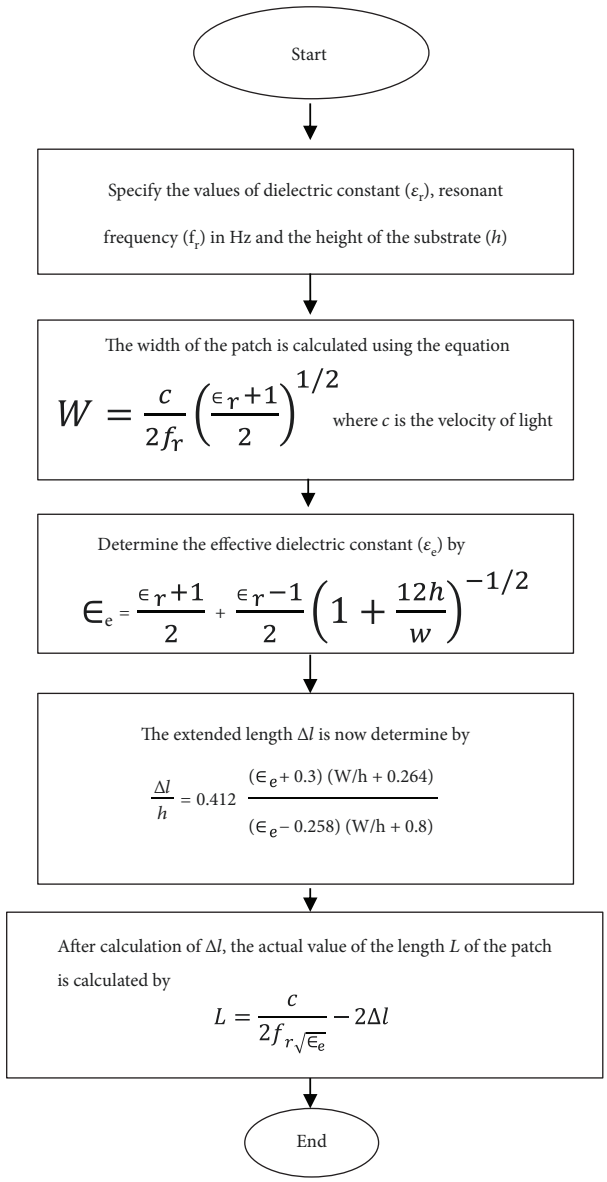

Figure 13: Design methodology for patch antenna.

K is the complete elliptic integral of the first kind and is given by Equation (9):

$$k = \frac{s}{s+2u}. \tag{9}$$

Using the above equations, C is 14.15×10^{-7} F.

The resultant impedance of the circuit in Figure 12 is given by Equation (10):

$$Z = sL + R1 + \frac{1}{sC + R2}, \tag{10}$$

where $s = j\omega$ and $\omega = 2\pi f$ where f is the resonant frequency.

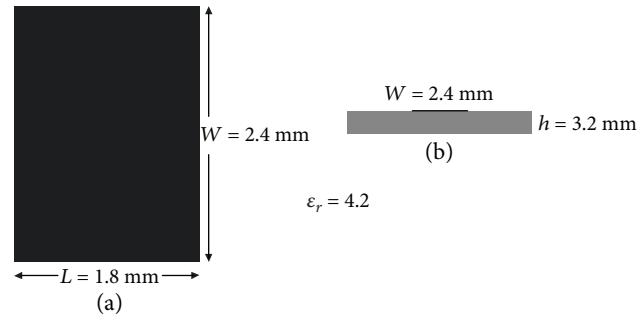

Figure 14: (a) Top view and (b) side view of the designed rectangular microstrip patch antenna.

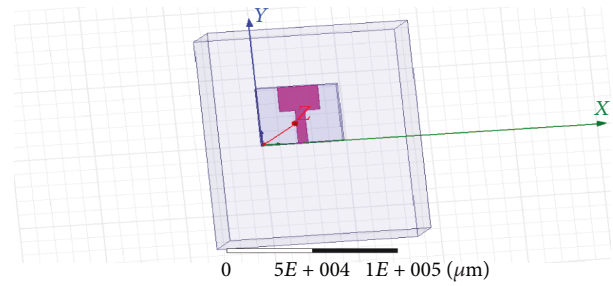

Figure 15: Rectangular microstrip patch antenna.

The frequency domain equivalent of Z is obtained by substituting $j\omega$ in place of s in Equation (10) and is given by Equation (11):

$$Z = j\omega L + R1 + \frac{1}{j\omega C + R2}. \tag{11}$$

At resonance, the imaginary part of Z is zero. So, Equation (11) becomes:

$$j\omega L + \frac{j\omega C}{-\omega^2 C^2 - R2^2} = 0. \tag{12}$$

Neglecting $R2$, the value of ω is given by Equation (13):

$$\omega = \sqrt{\frac{1}{L \cdot C}}. \tag{13}$$

Substituting the values of L and C in Equation (13), the resonant frequency is given as 4.08 GHz. Thus, around 1% error is seen between the simulation and the theoretical study of 2-segment SRR.

5. Antenna Design

A rectangular microstrip patch antenna is designed for 4.12 GHz as per the methodology shown in Figure 13 with design parameters as shown in Figure 14; the dielectric constant of the substrate is 4.2, FR4, and the thickness of the substrate is 3.2 mm.

The rectangular patch is etched on one side of the substrate, and the other side of the substrate acts as the ground plane. This whole antenna is excited by a quarter

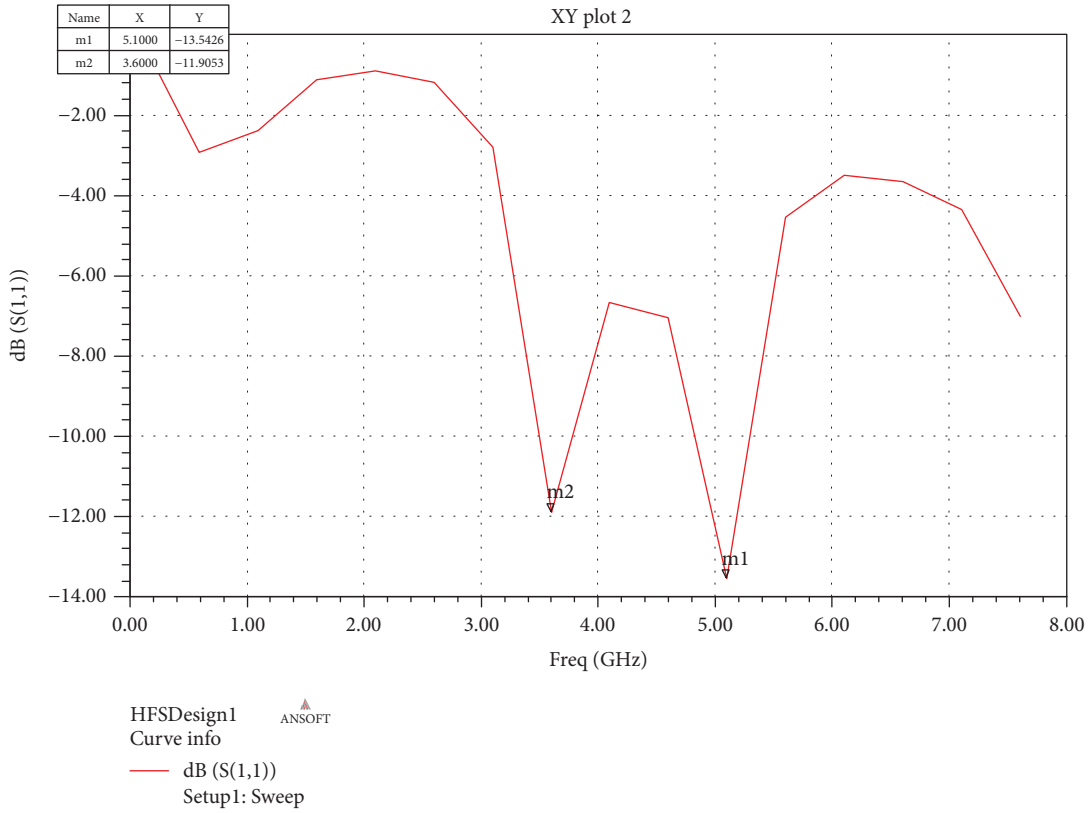

(a)

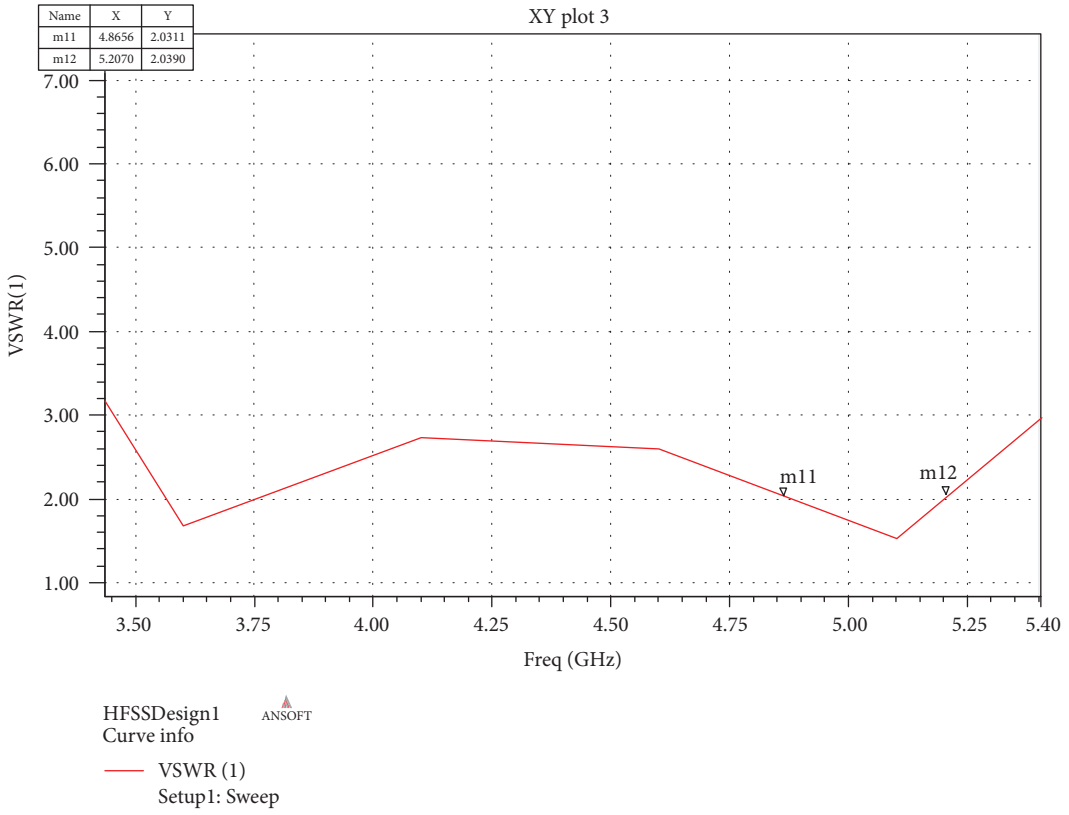

(b)

Figure 16: Continued.

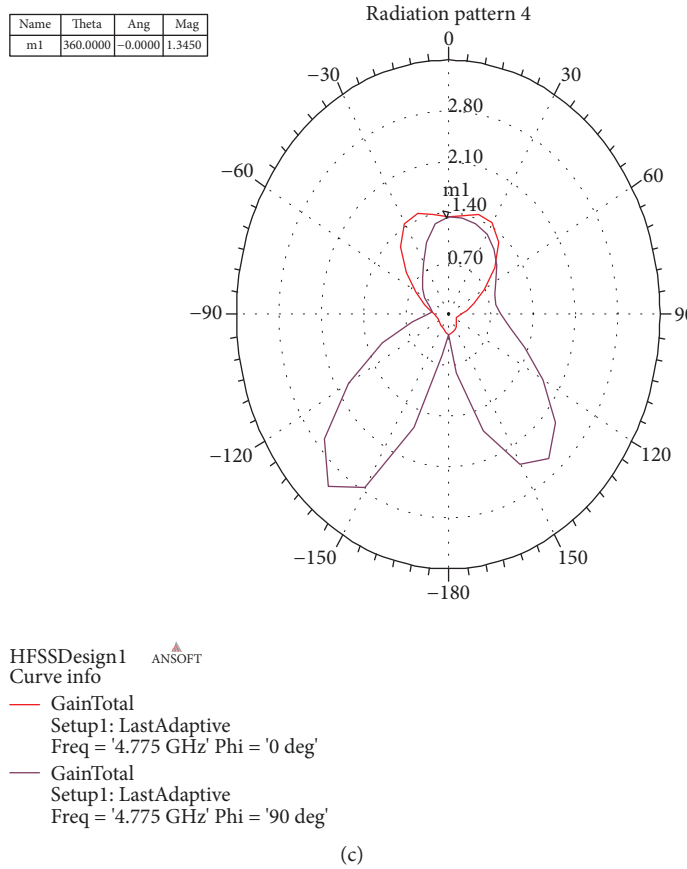

(c)

Figure 16: Simulation results of antenna for 2-segment labyrinth: (a) return loss, (b) VSWR, and (c) radiation pattern in E and H planes of RMPA.

Table 1: Various parameters of RMPA at 4.775 GHz.

Parameters	RMPA
S_{11} (dB)	−13.5
VSWR	1.49
Bandwidth (GHz)	0.4
E plane gain in dB	5.8
Peak directivity (dB)	4.6

wave-transformed matched microstrip feed as shown in Figure 15.

The patch is simulated using Ansoft HFSS software, and the simulation results of the different performance parameters of antenna are shown in Figure 16.

The above simulation results are tabulated in Table 1.

For this antenna, the return loss is −13.5 with VSWR of 1.49. This shows that the impedance matching of the antenna is within the limits. The bandwidth of the antenna is 0.4 GHz. To improve the performance parameters of the above antenna, the structure of this conventional rectangular patch is modified by embedding a 2-segment labyrinth metamaterial in the middle of the substrate. This metamaterial is embedded in the middle of the antenna's substrate such that the center of patch coincides with the center of the metamaterial. The structure is then simulated using HFSS software.

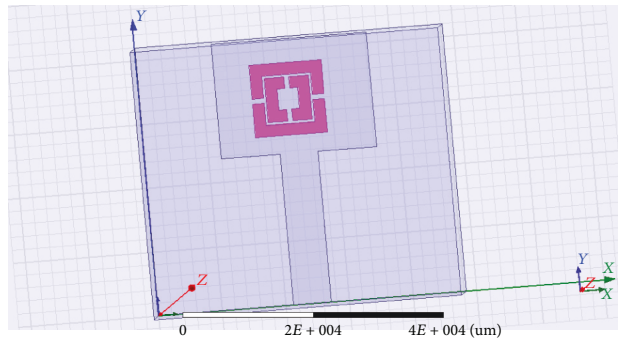

Figure 17: Top view of 2-segment SRR metamaterial RMPA.

The top view of the 2-segment SRR metamaterial RMPA is shown in Figure 17.

The study of performance parameters is shown in the simulation of this designed 2-segment SRR metamaterial RMPA shown in Figure 18.

The performance parameters of the MTM RMPA are shown in Table 2.

By comparing Tables 1 and 2, it can be observed that by embedding a 2-segment labyrinth metamaterial in the middle of the substrate of the patch antenna, the bandwidth increases by 6 times, in the GHz range. This lowers the effective permittivity of the antenna's substrate, which

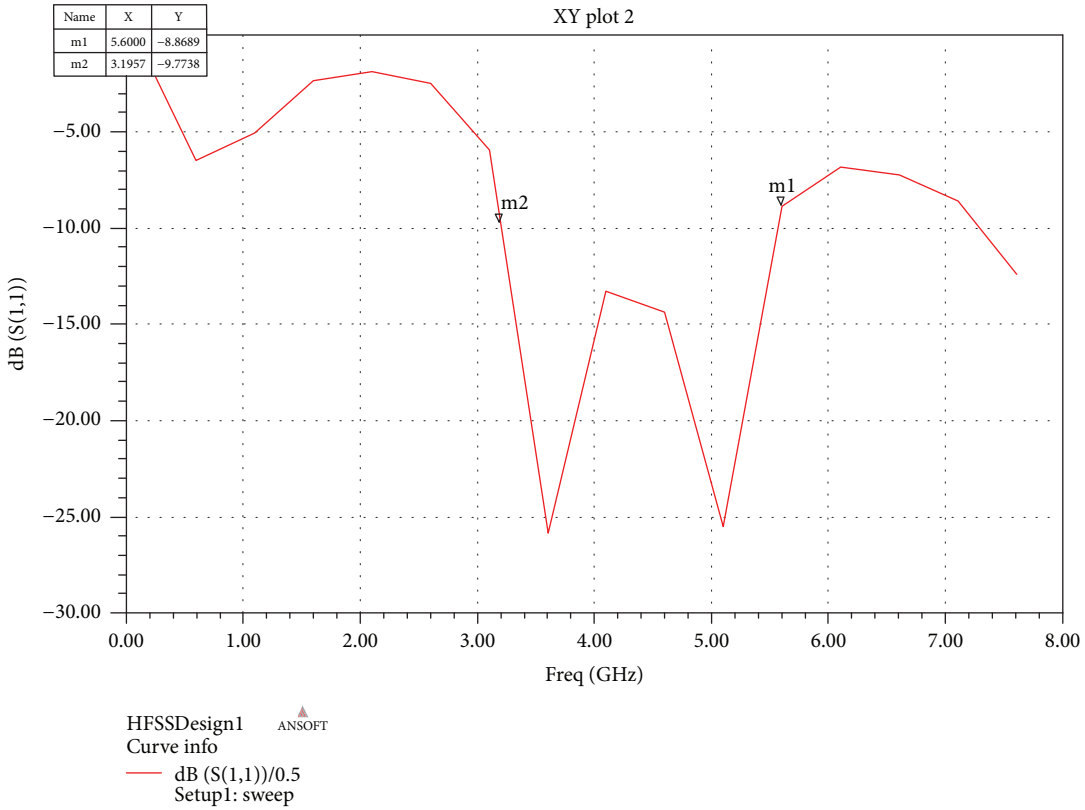

(a)

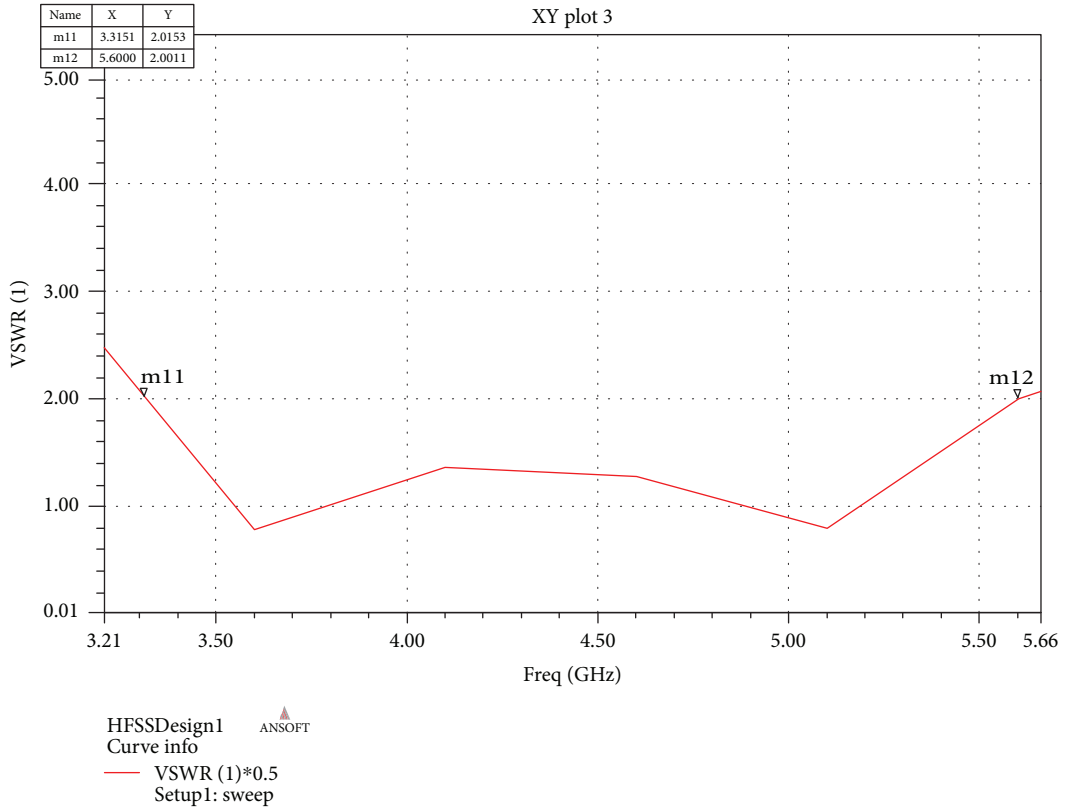

(b)

Figure 18: Continued.

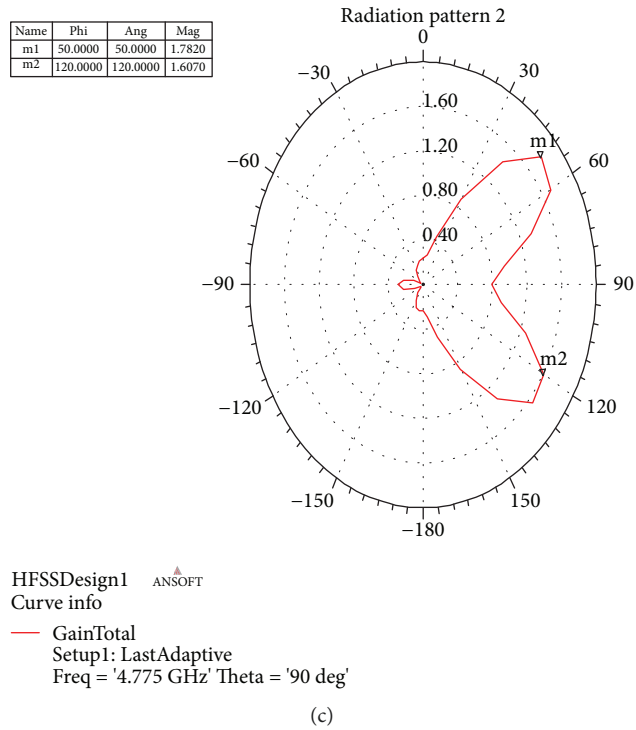

(c)

Figure 18: Simulation results for 2-segment SRR metamaterial RMPA: (a) return loss, (b) VSWR, and (c) radiation pattern in E and H planes.

Table 2: Various parameters of labyrinth MTM embedded in RMPA substrate.

Antenna/parameters	RMPA with labyrinth MTM
S_{11} (dB)	−25
VSWR	1.26
Bandwidth	2.3
E plane gain dB	3.18

(a) (b)

Figure 19: Fabricated antenna: microstrip patch antenna: (a) top view and (b) bottom view.

leads to a spreading of the electric field. This in turn leads to broadening of the bandwidth. Improvement in VSWR by 1.5% indicates better impedance matching of the antenna when it is loaded with the metamaterial than conventional patch antenna. However, the trade-off is reduction in gain by 1.5%. This is because the product of gain and bandwidth

Figure 20: Keysight Fieldfox RF Network Analyzer.

is unity. So, in this structure, gain decreases due to an increase in bandwidth. It can be seen that the miniaturization of nearly $1/4^{th}$ of the conventional patch is obtained as secondary resonance is observed at 3.19 GHz.

The proposed antenna operates at the C-band, which is used in satellite applications and is more compact and broadband than the actual antenna that would be designed at C-band frequencies.

6. Experimental Validation of Simulated Results

This rectangular microstrip patch antenna has been fabricated on FR4 substrate. The fabricated antenna is shown in Figure 19.

Using the Keysight Fieldfox RF Network Analyzer as shown in Figure 20, the simulation and fabrication results are compared in Figure 21.

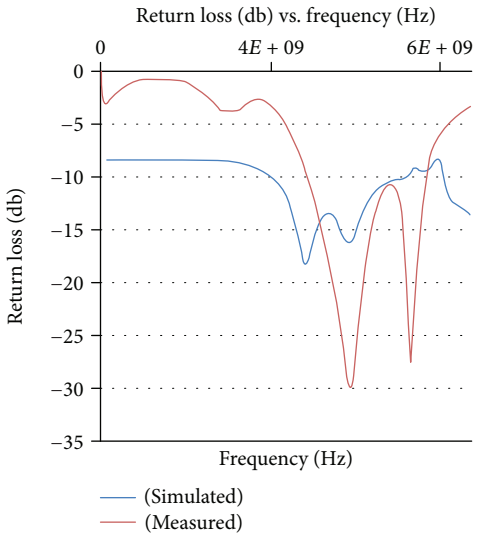

Figure 21: Return loss of patch antenna.

Figure 22: AMITECH gain measurement set-up.

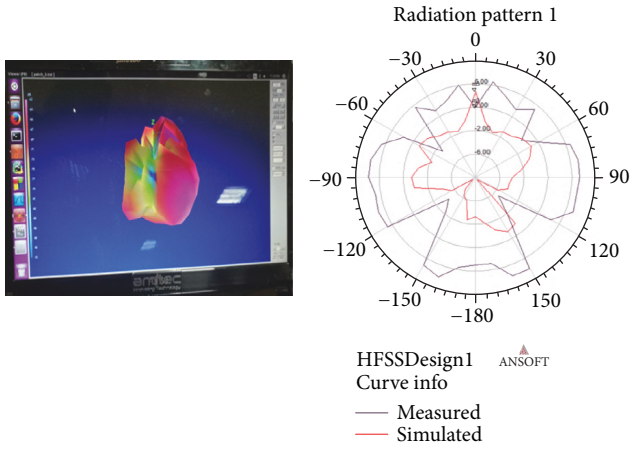

Figure 23: Radiation pattern measurement of patch antenna.

Using AMITECH, the gain measurement set-up is as shown in Figure 22.

Using the gain measurement set-up, a radiation pattern is obtained as in Figure 23.

The patch antenna is fabricated by embedding a 2-segment SRR metamaterial in the middle of the substrate as shown in Figure 24.

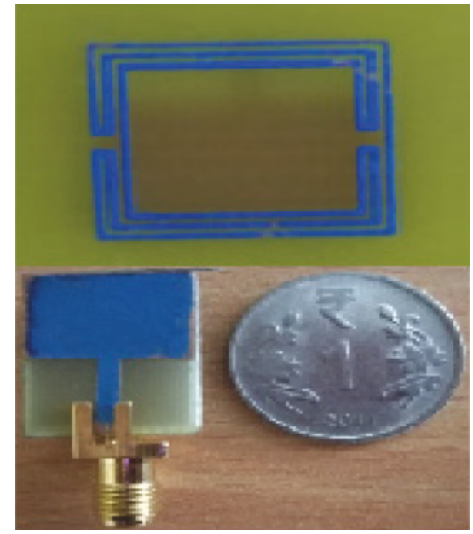

Figure 24: Fabricated antennas: microstrip patch antenna.

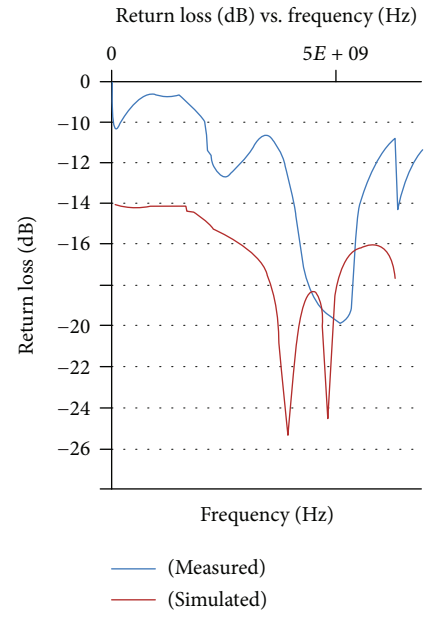

Figure 25: Return loss of metamaterial patch antenna.

Using the Keysight Fieldfox RF Network Analyzer as shown in Figure 20, the simulation and fabrication results are compared in Figure 25.

Thus, "fabricated and simulated antennas" help in achieving miniaturization and bandwidth enhancement which is in coherence with the proposed antenna configurations with nearly 5% error. It is normal to have some differences between simulated and measured results because of the following reasons:

(a) Fabrication tolerances (e.g., SMA soldering) and measurement error/limitations

(b) In simulation, when the substrate is selected, it shows a perfect material; however, variations in

Table 3: Comparison results of 2-segment SRR MTM in RMPA substrate with literature.

Reference no.	% Improvement in bandwidth of MPA	% Miniaturization
[17]	−5%	4%
[18]	−2%	24%
[19]	43.6%	41%
[20]	78.5%	4%
Proposed configuration	600%	25%

thickness & dielectric constant exist in commercially available material (especially the latter which has more influence).

(c) In actual measurement, i.e., if measurement is done inside a room/lab, there may be a lot of metallic objects which will highly affect results due to limited surrounding reflection phenomena. The influence could be on a worst side or best side; i.e., depending upon reflected signal, it can be either additive or subtractive.

In literature [17–20], using 2-segment SRRs, the bandwidth of the patch antenna is reduced, but 24% miniaturization is obtained. However, using 2-segment SRR in the middle of the antenna's substrate, an increase in the bandwidth by 600% and miniaturization of nearly 1/4th, i.e., 25% of the conventional patch, is obtained as secondary resonance is observed at 3.19 GHz. Thus, the proposed configuration is better than the previous configurations in literature. The findings can be tabulated as shown in Table 3.

7. Conclusion

In this paper, a proposed novel microstrip antenna attains miniaturization by nearly 400% and maximization in bandwidth of nearly 600% with metamaterial embedded in the middle of the substrate of the patch antenna. This is a result of negative permeability of the metamaterial which reduces the effective medium below the patch.

Data Availability

The data used to support the findings of this study are available from the corresponding author upon request.

Conflicts of Interest

The authors declare that they have no conflicts of interest.

References

[1] J. B. Pendry, A. J. Holden, D. J. Robbins, and W. J. Stewart, "Magnetism from conductors and enhanced nonlinear phenomena," *IEEE Transactions on Microwave Theory and Techniques*, vol. 47, no. 11, pp. 2075–2084, 1999.

[2] B. Ferguson and X.-C. Zhang, "Materials for terahertz science and technology," *Nature Materials*, vol. 1, no. 1, pp. 26–33, 2002.

[3] D. R. Chowdhury, R. Singh, M. Reiten, J. Zhou, A. J. Taylor, and J. F. O'Hara, "Tailored resonator coupling for modifying the terahertz metamaterial response," *Optics Express*, vol. 19, no. 11, pp. 10679–10685, 2011.

[4] C. Caloz and T. Itoh, "Metamaterials for high-frequency electronics," *Proceedings of the IEEE*, vol. 93, no. 10, pp. 1744–1752, 2005.

[5] R. P. Clayton, *Inductance: Loop and Partial*, Wiley, Hoboken, NJ, USA, 2009.

[6] R. E. Collins, *Foundations for Microwave Engineering*, McGraw-Hill Book Company, New York, NY, 1966.

[7] D. Hyun Lee, A. Chauraya, Y. Vardaxoglou, and W. S. Park, "A compact and low-profile tunable loop antenna integrated with inductors," *IEEE Antennas and Wireless Propagation Letters*, vol. 7, pp. 621–624, 2008.

[8] D. Psychoudakis, Y. H. Koh, J. L. Volakis, and J. H. Halloran, "Design method for aperture-coupled microstrip patch antennas on textured dielectric substrates," *IEEE Transactions on Antennas and Propagation*, vol. 52, no. 10, pp. 2763–2765, 2004.

[9] D. R. Smith, S. Schultz, P. Markoš, and C. M. Soukoulis, "Determination of effective permittivity and permeability of metamaterials from reflection and transmission coefficients," *Physical Review B*, vol. 65, no. 19, article 195104, 2002.

[10] D. R. Smith, J. B. Pendry, and M. C. Wiltshire, "Metamaterials and negative refractive index," *Science*, vol. 305, no. 5685, pp. 788–792, 2004.

[11] C. T. Chan, S. Datta, Q. L. Yu, M. Sigalas, K. M. Ho, and C. M. Soukoulis, "New structures and algorithms for photonic band gaps," *Physica A: Statistical Mechanics and its Applications*, vol. 211, no. 4, pp. 411–419, 1994.

[12] C. Caloz and T. Itoh, *Electromagnetic Metamaterials: Transmission Line Theory and Techniques*, Wiley, 2006.

[13] H. Schantz, *The Art and Science of Ultra-Wide Band Antennas*, Artech House, 2005.

[14] B. Danana, B. Choudhury, and R. M. Jha, "Design of high gain microstrip antenna for THz wireless communication," *International Journal of Advanced Research in Electrical, Electronics and Instrumentation Engineering*, vol. 3, no. 5, pp. 711–716, 2014.

[15] O. Paul, C. Imhof, B. Reinhard, R. Zengerle, and R. Beigang, "Negative index bulk metamaterial at terahertz frequencies," *Optical Society of America*, vol. 16, no. 9, pp. 6736–6744, 2008.

[16] G. Kiziltas and J. L. Volakis, "Miniature antenna designs on metamaterial substrates," in *8th Int. Conference on Electromagnetics in Advanced Appl. (ICEAA), Conf. Proceedings*, pp. 431–434, Torino, Italy, 2003.

[17] N. Abdullah and G. Bhardwaj, "Design of squared shape SRR metamaterial by using rectangular microstrip patch antenna at 2.85 GHz," in *2017 4th International Conference on Signal Processing and Integrated Networks (SPIN)*, pp. 196–200, Amity University, Noida, Delhi, February 2017.

[18] S. Kar, M. Ghosh, A. Kumar, and A. Majumder, "Complementary split ring resonator-loaded microstrip patch antenna useful for microwave communication," *World Academy of Science, Engineering and Technology, International Journal of Electrical, Computer, Energetic, Electronic and Communication Engineering*, vol. 10, no. 10, pp. 1321–1325, 2016.

[19] L. Peng, P. Chen, A. Wu, and G. Wang, "Efficient radiation by electrically small antennas made of coupled split-ring resonators," *Scientific Reports*, vol. 6, no. 1, 2016.

[20] D. Chaturvedi and S. Raghavan, "SRR-loaded metamaterial-inspired electrically-small monopole antenna," *Progress In Electromagnetics Research C*, vol. 81, pp. 11–19, 2018.